ARCHIVES OF MECHANICS
Arch. Mech. **74** (2-3), 89–108, 2022, DOI: 10.24423/aom.3957

Nonlinear postbuckling behavior of auxetic-core toroidal shell segments with Graphene reinforced face sheets under axial loads

V. H. NAM, V. M. DUC, C. V. DOAN,
N. T. THANH XUAN, N. T. PHUONG

Faculty of Civil Engineering, University of Transport Technology, Hanoi 100000, Vietnam, email: hoainam.vu@utt.edu.vn

The main aim of this paper is to provide an analytical approach for the nonlinear buckling behaviors of toroidal shell segments made by three layers included honeycomb auxetic-core and two Graphene reinforced face sheets under axial compressive or tensile loads. The auxetic core is designed in a honeycomb form and three distribution laws of Graphene are considered for two symmetric face sheets. The homogenization technique for honeycomb auxetic plates and shells is applied to establish the stiffness formulations of the core. By approximating the doubly curved coordinate to the simpler coordinate with the Stein and McElman assumption, the nonlinear basic equations are formulated using the nonlinear Donnell shell theory and the model of the two-parameter foundation. The Galerkin method can be performed three times for three states of buckling responses and the expressions of the load-deflection postbuckling curves can be determined. The numerical examinations present that the bifurcation buckling occurs with both axial tensile and compressive loads for convex and concave shells and the significantly beneficial effects of auxetic core and functionally graded Graphene reinforced face sheets on nonlinear buckling responses of shell segments.

Key words: axial compressive or tensile load, nonlinear buckling, graphene reinforced composite, auxetic-core, face sheet, toroidal shell segment.

1. Introduction

The toroidal shell segments are the popular form of the shell of revolution with double curvature in the circumferential and longitudinal direction [1]. In the case of zero longitudinal curvature, another special form that can be obtained is the cylindrical shell. In general, the toroidal shell segments and cylindrical shells are widely applied in industries. The use of advanced materials for these structures provides a great bearing capacity accompanied by an interesting mechanical behavior. This is also a great motivation for researchers to make publications on the mechanical behavior of these structures made of various composite materials.

The functionally graded ceramic/metal material (FGM) [2] is the first in the family of functionally graded materials. Therefore, in the last decade, analyzing the mechanical behavior of ceramic/metal FGM cylindrical shells and toroidal shell segments has become a hot topic. The static buckling and nonlinear postbuckling responses of FGM cylindrical shells were investigated with axial compression [3], with inelastic material properties [4], with dynamic loads [5], and with thermal loads [6]. The dynamic behavior of FGM toroidal shell segments was presented [7] and the vibration problem of FGM conical shells was also investigated [8]. The orthogonally and spirally stiffened FGM cylindrical shells were mentioned for nonlinear static buckling under different load types [9, 10] and the full-filled fluid corrugated FGM cylindrical shells were also investigated for nonlinear vibration [11].

The new transcendent material is a carbon nanotube (CNT) with nanoscale, it is an excellent candidate to reinforce matrix materials in the macroscale to form a new composite material with special properties [12]. The isotropic polymer matrix can be reinforced by CNT respecting a continuous function of the CNT volume fraction, Shen [13, 14] presented a new functionally graded composite, called functionally graded CNT-reinforced composite (FG-CNTRC). Static buckling analysis of FG-CNTRC cylindrical shells and panels were studied using different methods, with two-step perturbation method [13, 14], kp-Ritz method [15], and meshless method [16]. The dynamic behavior of CNT-reinforced cylindrical panels [17] and cylindrical shells [18] was studied and the static buckling of toroidal shell segments reinforced by CNT in two orthogonal directions of shells was investigated [19].

Another transcendent material with another allotropic form of carbon is Graphene [20]. With the two-dimensional form of the honeycomb lattice of carbon atoms, Graphene sheets provide a better bond with the matrix material. A new nanocomposite material called functionally graded graphene reinforced composite was designed with the piecewise function distributed laws of Graphene volume fraction [21]. Nonlinear bending [21], mechanical buckling and postbuckling [22–25], thermal postbuckling [26], and nonlinear vibration [27] of FG-GRC laminated plates and cylindrical shells and conical shells were mentioned. Postbuckling analysis of FG-GRC laminated toroidal shell segments was studied with the shell-foundation interaction of Pasternak's model [28]. The improved smeared stiffener technique is presented to model the behavior of FG-GRC laminated stiffeners of FG-GRC laminated cylindrical shells [29–31].

With the negative Poisson's ratio and the low density, the auxetic-core structures are known as a light material and excellent in absorbing impact impulses. For static problems, the auxetic core is used as a light core that increases the total stiffnesses of structures. The mechanical behavior of auxetic-core structures becomes a particularly exciting topic with interesting and unusual results. In recent

years, many publications have focused on the mechanical behavior of shell-plate structures with face coatings made of different materials with auxetic cores [32–38].

The current paper analyses the nonlinear axial compressive and tensile buckling behavior of the convex and concave sandwich toroidal shell segments with the GRC face sheets and auxetic core considering Pasternak's shell-foundation interactions. The governing equations are established using the nonlinear Donnell shell theory and the Stein and McElman assumption [1]. The stress function is introduced and the Galerkin procedure is applied to obtain the nonlinear equilibrium equations in the algebraic form. The large effects of the auxetic core, foundation, geometrical and material properties on the buckling and postbuckling behavior of sandwich toroidal shell segments are investigated in numerical examples.

2. Shell's configuration, mechanical characteristics of core and face sheets

Consider the sandwich toroidal shell segments with the auxetic core and shallow curvature in longitudinal direction under axial compressive or tensile load denoted as r_0(in Pa) (see Fig. 1). The axial load is uniformly distributed over the area of the two ends of the shell. As can be seen in Fig. 1, the toroidal shell seg-

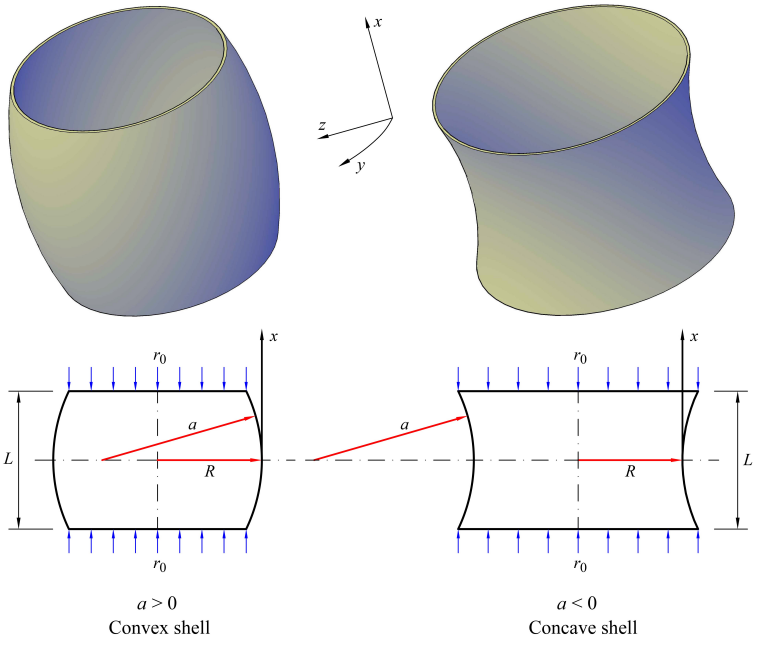

FIG. 1. Configuration, coordinate system and geometrical properties of toroidal shell segments.

ments are characterized by the length L, the radius in the longitudinal direction a, and the radius in the circumferential direction R. In this paper, the governing equations are established where R is always positive, $a > 0$ corresponds to the convex shell, $a < 0$ corresponds to the concave shell, and $a = \infty$ corresponds to the cylindrical shell.

The shells are constructed from two Graphene reinforced face sheets and the honeycomb auxetic core made from matrix material of GRC with h is the total thickness of the layers. The geometrical dimensions of GRC face sheets, and of auxetic core can be seen in Fig. 2. Note also that the darker layers represent more graphene in the GRC layers. In this paper, the graphene volume fractions for three distributed laws UD, FG-X, and FG-O and the graphene arrangements in the layers are applied according to [21–23]. The graphene volume fractions of 5 layers of GRC face sheets from the outer layer to the inner layer are [0.11/0.09/0.07/0.05/0.03] for FG-X law, are [0.03/0.05/0.07/0.09/0.11] for FG-O law, and are [0.07/0.07/0.07/0.07/0.07] for UD law.

The orthotropic elastic moduli and shear modulus of GRC layers are predicted using the Halpin–Tsai model, expressed as [21–23]

$$
\begin{aligned}
E_1^{\mathrm{GRC}} &= \eta_1 \frac{1 + 2(a_{\mathrm{Gra}}/h_{\mathrm{Gra}})\gamma_1^{\mathrm{Gra}} V_{\mathrm{Gra}} E_{\mathrm{ma}}}{1 - \gamma_1^{\mathrm{Gra}} V_{\mathrm{Gra}}}, \\
E_2^{\mathrm{GRC}} &= \eta_2 \frac{1 + 2(b_{\mathrm{Gra}}/h_{\mathrm{Gra}})\gamma_2^{\mathrm{Gra}} V_{\mathrm{Gra}} E_{\mathrm{ma}}}{1 - \gamma_2^{\mathrm{Gra}} V_{\mathrm{Gra}}}, \\
G_{12}^{\mathrm{GRC}} &= \eta_3 \frac{G_{\mathrm{ma}}}{1 - \gamma_{12}^{\mathrm{Gra}} V_{\mathrm{Gra}}},
\end{aligned}
\tag{2.1}
$$

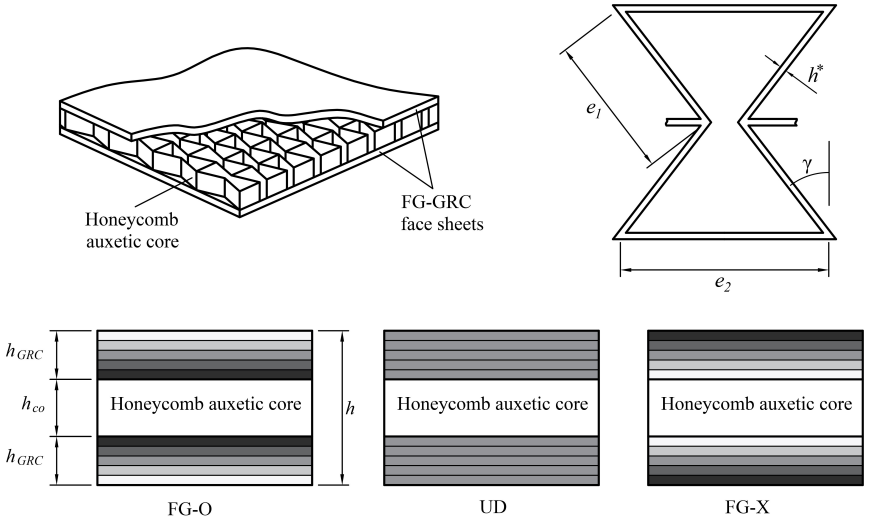

FIG. 2. Configurations of auxetic core and distribution laws of GRC face sheets.

with

$$\gamma_1^{\mathrm{Gra}} = \frac{E_{11}^{\mathrm{Gra}}/E_{\mathrm{ma}} - 1}{E_{11}^{\mathrm{Gra}}/E_{\mathrm{ma}} + 2a_{\mathrm{Gra}}/h_{\mathrm{Gra}}},$$
$$\gamma_2^{\mathrm{Gra}} = \frac{E_{22}^{\mathrm{Gra}}/E_{\mathrm{ma}} - 1}{E_{22}^{\mathrm{Gra}}/E_{\mathrm{ma}} + 2b_{\mathrm{Gra}}/h_{\mathrm{Gra}}}, \tag{2.2}$$
$$\gamma_{12}^{\mathrm{Gra}} = \frac{G_{12}^{\mathrm{Gra}}/G_{\mathrm{ma}} - 1}{G_{12}^{\mathrm{Gra}}/G_{\mathrm{ma}}},$$

where a_{Gra}, b_{Gra} are respectively the length, width, and h_{Gra} is the effective thickness of graphene sheet. $E_{11}^{\mathrm{Gra}}, E_{22}^{\mathrm{Gra}}, G_{12}^{\mathrm{Gra}}$ and $E_{\mathrm{ma}}, G_{\mathrm{ma}}$ are respectively, the elastic moduli and shear moduli of graphene sheet and matrix. V_{Gra} and V_{ma} are the graphene and matrix volume fractions, respectively, note that $V_{\mathrm{Gra}}+V_{\mathrm{ma}} = 1$. The graphene efficiency parameters η_j $(j = 1, 2, 3)$ depend to the graphene volume fraction V_{Gra} [21–23].

The orthotropic elastic moduli, shear modulus and orthotropic Poisson's ratios of the honeycomb auxetic core layers can be estimated by applying a homogeneous technique for auxetic structure, as [33]

$$E_1^{\mathrm{Auxetic}} = E_{\mathrm{ma}} \frac{\chi_2^3(\chi_1 - \sin\gamma)}{\cos^3\gamma[(\chi_1 \sec^2\gamma + \tan^2\gamma)\chi_2^2 + 1]},$$
$$E_2^{\mathrm{Auxetic}} = E_{\mathrm{ma}} \frac{\chi_2^3}{(\chi_1 - \sin\gamma)(\tan^2\gamma + \chi_2^2)\cos\gamma},$$
$$G_{12}^{\mathrm{Auxetic}} = E_{\mathrm{ma}} \frac{\chi_2^3}{(1 + 2\chi_1)\chi_1 \cos\gamma}, \tag{2.3}$$
$$\nu_{12}^{\mathrm{Auxetic}} = -\frac{(1 - \chi_2^2)\sin\gamma(\chi_1 - \sin\gamma)}{[(\chi_1 \sec^2\gamma + \tan^2\gamma)\chi_2^2 + 1]\cos^2\gamma},$$
$$\nu_{21}^{\mathrm{Auxetic}} = \frac{(\chi_2^2 - 1)\sin\gamma}{(\chi_1 - \sin\gamma)(\tan^2\gamma + \chi_2^2)},$$

where $\chi_1 = e_2/e_1$, $\chi_2 = h^*/e_1$.

In Fig. 1, as can be observed, the shell has two curvatures in longitudinal and circumferential directions. For a sufficiently shallow toroidal shell in the longitudinal direction, i.e. the radius a is sufficiently large, STEIN and MCELMAN [1] assume that the radius in the circumferential direction of the shell is constant throughout the longitudinal direction of the shell and is equal to R. This doubly curved coordinate system can be approximated to a simpler coordinate system. The geometrically nonlinear Donnell shell theory is employed to formulate the governing equations of buckling responses of shells under axial compressive or

tensile loads. The nonlinear relations of the strain-displacement are presented, as [39]

$$\begin{aligned}\varepsilon_x^0 &= u_{,x} + \frac{w_{,x}^2}{2} - \frac{w}{a},\\ \varepsilon_y^0 &= v_{,y} + \frac{w_{,y}^2}{2} - \frac{w}{R},\\ \gamma_{xy}^0 &= u_{,y} + v_{,x} + w_{,x}w_{,y},\end{aligned} \tag{2.4}$$

where ε_x^0, ε_y^0, γ_{xy}^0 denote the mid-plane strains, u, v, and w are the displacements in x, y and z directions, respectively, R and a are the radii in the circumferential and longitudinal directions, respectively.

The elastic linear Hooke's law of orthotropic plates or shells applied for the considered toroidal shell segments is written as

$$\sigma_x = Q_{11}\varepsilon_x + Q_{12}\varepsilon_y, \quad \sigma_y = Q_{22}\varepsilon_y + Q_{12}\varepsilon_x, \quad \sigma_{xy} = Q_{66}\gamma_{xy}, \tag{2.5}$$

where

$$Q_{11} = \frac{E_1}{1-\nu_{21}\nu_{12}}, \quad Q_{12} = \frac{E_1\nu_{21}}{1-\nu_{21}\nu_{12}}, \quad Q_{22} = \frac{E_2}{1-\nu_{21}\nu_{12}}, \quad Q_{66} = G_{12},$$

with E_1, E_2 are the orthotropic elastic moduli, G_{12} is the shear modulus and ν_{12}, ν_{21} are the orthotropic Poisson's ratios of the shells.

The forces and moments of toroidal shell segments with GRC face sheets are presented, as:

$$\begin{aligned}N_x &= A_{11}^{\text{sum}}\varepsilon_x^0 + A_{12}^{\text{sum}}\varepsilon_y^0 - B_{11}^{\text{sum}}w_{,xx}, \quad N_{xy} = A_{66}^{\text{sum}}\gamma_{xy}^0,\\ N_y &= A_{12}^{\text{sum}}\varepsilon_x^0 + A_{22}^{\text{sum}}\varepsilon_y^0 - B_{22}^{\text{sum}}w_{,yy},\\ M_x &= B_{11}^{\text{sum}}\varepsilon_x^0 - D_{11}^{\text{sum}}w_{,xx} - D_{12}^{\text{sum}}w_{,yy}, \quad M_{xy} = -2D_{66}^{\text{sum}}w_{,xy},\\ M_y &= B_{22}^{\text{sum}}\varepsilon_y^0 - D_{12}^{\text{sum}}w_{,xx} - D_{22}^{\text{sum}}w_{,yy},\end{aligned} \tag{2.6}$$

where A_{ij}^{sum}, B_{ij}^{sum}, D_{ij}^{sum} are the sum stiffnesses of shells, determined by summing the stiffnesses of two GRC face sheets and auxetic core, respectively.

Note that: by summing the stiffnesses of the layers, respectively, the auxetic-core shell with GRC face sheets is homogenized into an equivalent shell that is characterized by the sum stiffnesses A_{ij}^{sum}, B_{ij}^{sum}, D_{ij}^{sum}.

3. Nonlinear equilibrium equations

The compatibility equation of considered toroidal shell segments is established by employing Eq. (2.4), as [39]

$$\varepsilon_{x,yy}^0 + \varepsilon_{y,xx}^0 - \gamma_{xy,xy}^0 - w_{,xy}^2 + w_{,xx}/R + w_{,yy}/a + w_{,xx}w_{,yy} = 0. \tag{3.1}$$

The equilibrium equation system of considered shells combining the shell-foundation interaction within the nonlinear thin shell theory are expressed as [39]

$$
\begin{aligned}
&N_{x,x} + N_{xy,y} = 0, \quad N_{xy,x} + N_{y,y} = 0,\\
&M_{x,xx} + M_{y,yy} + 2M_{xy,xy} + N_x w_{,xx} + N_y w_{,yy} + 2N_{xy} w_{,xy}\\
&\qquad + \frac{N_x}{a} + \frac{N_y}{R} - K_W w + K_P(w_{,xx} + w_{,yy}) = 0,
\end{aligned} \tag{3.2}
$$

where K_W and K_P are foundation parameters in Pasternak's model.

An assumption is made here that an introduced stress function $\xi(x, y)$ satisfies the conditions

$$
N_x = \xi_{,yy}, \quad N_{xy} = -\xi_{,xy}, \quad N_y = \xi_{,xx}. \tag{3.3}
$$

Two first equations of (3.2) are completely satisfied if three conditions of Eq. (3.3) are ensured the governing equations are reduced to two-equation system including the last equilibrium equation of (3.2) and the compatibility equation (3.1), rewritten as

$$
\begin{aligned}
&Y_1 w_{,xxxx} + Y_2 w_{,xxyy} + Y_3 w_{,yyyy} - Y_4 \xi_{,xxyy} - w_{,xx}\xi_{,yy} - w_{,yy}\xi_{,xx}\\
&\qquad + 2w_{,xy}\xi_{,xy} - \frac{1}{R}\xi_{,xx} - \frac{1}{a}\xi_{,yy} = -K_W w + K_P(w_{,xx} + w_{,yy}),
\end{aligned} \tag{3.4}
$$

$$
\begin{aligned}
&X_1 \xi_{,xxxx} + X_2 \xi_{,xxyy} + X_3 \xi_{,yyyy} + X_4 w_{,xxyy} + w_{,xx} w_{,yy}\\
&\qquad + \frac{w_{,xx}}{R} + \frac{w_{,yy}}{a} - w_{,xy}^2 = 0,
\end{aligned} \tag{3.5}
$$

where

$$
\begin{aligned}
&X_1 = \frac{A_{11}^{\text{sum}}}{A_{11}^{\text{sum}} A_{22}^{\text{sum}} - (A_{12}^{\text{sum}})^2}, \quad X_2 = \frac{1}{A_{66}^{\text{sum}}} - \frac{2A_{12}^{\text{sum}}}{A_{11}^{\text{sum}} A_{22}^{\text{sum}} - (A_{12}^{\text{sum}})^2},\\
&X_3 = \frac{A_{22}^{\text{sum}}}{A_{11}^{\text{sum}} A_{22}^{\text{sum}} - (A_{12}^{\text{sum}})^2}, \quad X_4 = Y_4,\\
&Y_1 = D_{11}^{\text{sum}} - \frac{A_{22}^{\text{sum}} (B_{11}^{\text{sum}})^2}{A_{11}^{\text{sum}} A_{22}^{\text{sum}} - (A_{12}^{\text{sum}})^2}, \quad Y_2 = 2D_{12}^{\text{sum}} + 4D_{66}^{\text{sum}},\\
&Y_3 = D_{22}^{\text{sum}} - \frac{\hat{A}_{11} (B_{11}^{\text{sum}})^2}{A_{11}^{\text{sum}} A_{22}^{\text{sum}} - (A_{12}^{\text{sum}})^2}, \quad Y_4 = \frac{A_{22}^{\text{sum}} B_{11}^{\text{sum}} + A_{11}^{\text{sum}} B_{22}^{\text{sum}}}{A_{11}^{\text{sum}} A_{22}^{\text{sum}} - (A_{12}^{\text{sum}})^2}.
\end{aligned}
$$

Similarly with any types of revolution shells, the closed condition must be ensured, by using an average relation [3]

$$
\int_0^{2\pi R} \int_0^{L} v_{,y}\, dx\, dy = 0. \tag{3.6}
$$

Nonlinear axial compressive or tensile buckling of considered shells can be investigated by solving the nonlinear system (3.4)–(3.6).

4. Chosen solution of deflection and solution method

Consider a simply-supported toroidal shell segments made from three layers, including the auxetic core and Graphene reinforced face sheets subjected to axial compressive or tensile loads. Assuming that the chosen solution of deflection is approximately in the form [3]

$$w(x,y) = \kappa_{uf} + \kappa_{li}\sin\hat{M}x\sin\hat{N}y + \kappa_{nl}\sin^2\hat{M}x, \tag{4.1}$$

where $\hat{M} = m\pi/L$, $\hat{N} = n/R$, with the buckling modes are denoted respectively by m and n in the longitudinal and circumferential directions.

From Eq. (4.1), the maximum value of the total deflection is calculated by

$$W_{\max} = \kappa_{uf} + \kappa_{li} + \kappa_{nl}. \tag{4.2}$$

Substituting the deflection form (4.1) into Eq. (3.5) the stress function can be expressed in the explicit form as

$$\begin{aligned}\xi = {} & \xi_1\cos 2\hat{M} + \xi_2\cos 2\hat{N} - \xi_3\sin\hat{M}\sin\hat{N} \\ & + \xi_4\sin 3\hat{M}\sin\hat{N} - \sigma_y h\frac{x^2}{2} - r_0 h\frac{y^2}{2},\end{aligned} \tag{4.3}$$

where

$$\begin{aligned}
&\xi_1 = \kappa_{li}^2\frac{n^2\lambda^2}{32X_1m^2\pi^2} - \kappa_{nl}\frac{\lambda L}{8X_1m^2\pi^2}, \quad \xi_2 = \kappa_{li}^2\frac{m^2\pi^2}{32X_3n^2\lambda^2}, \\
&\xi_3 = \kappa_{li}\frac{\Xi_1}{\Gamma_1} + \kappa_{li}\kappa_{nl}\frac{m^2n^2\pi^2\lambda^2}{\Gamma_1}, \quad \xi_4 = \kappa_{li}\kappa_{nl}\frac{m^2n^2\pi^2\lambda^2}{\Phi_1}, \\
&\Gamma_1 = X_1m^4\pi^4 + X_3n^4\lambda^4 + X_2m^2n^2\pi^2\lambda^2, \\
&\Xi_1 = X_4m^2n^2\pi^2\lambda^2 - L^2m^2\pi^2/R - L^2n^2\pi^2/a, \\
&\Phi_1 = 81X_1m^4\pi^4 + X_3n^4\lambda^4 + 9X_2m^2n^2\pi^2\lambda^2, \quad \lambda = L/R.
\end{aligned}$$

Note that r_0 is positive for compressive load and negative for tensile load.

The deflection (4.1) and stress function (4.3) are substituted into Eq. (3.4) after that, the Galerkin procedure is applied. Combining these obtained equations with the closed condition (3.6), after a calculation process, the new forms of nonlinear algebraic equilibrium equations presented as

$$\kappa_{uf} = \frac{J_{32}}{2J_{31}}\kappa_{li}^2 - \frac{\kappa_{nl}}{2} - \frac{J_{34}}{2J_{31}}r_0, \tag{4.4}$$

$$J_{11} + J_{12}\kappa_{uf} + J_{13}\kappa_{li}^2 + J_{14}\kappa_{nl} + J_{15}\kappa_{nl}^2 - J_{16}r_0 = 0, \tag{4.5}$$

$$\kappa_{li}^2 = \frac{-J_{23}\kappa_{nl} + J_{24}\kappa_{nl}r_0}{J_{21} + J_{22}\kappa_{nl}}, \tag{4.6}$$

where

$$J_{11} = \Psi_1 + \frac{\Xi_1^2}{\Gamma_1} + L^4 K_W + L^2 K_P(\lambda^2 n^2 + m^2\pi^2),$$
$$J_{12} = n^2 L^2 \lambda^2 R K_W, J_{13} = \frac{m^4\pi^4}{16X_3} + \frac{n^4\lambda^4}{16X_1},$$
$$J_{14} = \frac{2\Xi_1 m^2 n^2 \pi^2 \lambda^2}{\Gamma_1} - \frac{n^2\lambda^3 L}{4X_1} + \frac{n^2 L^2 \lambda^2 R K_W}{2},$$
$$J_{15} = m^4 n^4 \pi^4 \lambda^4 \left(\frac{1}{\Gamma_1} + \frac{1}{\Phi_1}\right),$$
$$J_{16} = m^2\pi^2 L^2 h, \quad J_{21} = \frac{\Xi_1}{2\Gamma_1}\hat{M}^2\hat{N}^2 - \frac{\hat{M}^2 n^2 \lambda^2}{16 R L_1 m^2 \pi^2},$$
$$J_{22} = \frac{\hat{M}^2\hat{N}^2 m^2 n^2 \pi^2 \lambda^2}{2}\left(\frac{1}{\Gamma_1} - \frac{1}{\Phi_1}\right),$$
$$J_{23} = 4\hat{M}^4 Y_1 + \frac{\hat{M}^2}{R}\frac{\lambda L}{4m^2\pi^2 X_1} + \frac{K_W}{4} + K_P\hat{M}^2,$$
$$J_{24} = \hat{M}^2 h, J_{31} = \frac{1}{R} + X_1 R K_W, \quad J_{32} = \frac{\hat{N}^2}{4},$$
$$J_{34} = \frac{2hA_{12}^{\text{sum}}}{A_{11}^{\text{sum}} A_{22}^{\text{sum}} - (A_{12}^{\text{sum}})^2}, \quad \Psi_1 = Y_1 m^4\pi^4 + Y_3 n^4\lambda^4 + Y_2 m^2 n^2 \pi^2 \lambda^2.$$

Solving Eqs. (4.4)–(4.6), the relation of load-nonlinear amplitude can be determined, as

$$r_0 = \left[J_{11} + \left(J_{14} - \frac{J_{12}}{2}\right)\kappa_{nl} + J_{15}\kappa_{nl}^2 - \frac{J_{12}J_{23}J_{32}\kappa_{nl}}{2J_{31}(J_{21} + J_{22}\kappa_{nl})} - \frac{J_{13}J_{23}\kappa_{nl}}{J_{21} + J_{22}\kappa_{nl}}\right] \times \left(J_{16} + \frac{J_{12}J_{34}}{2J_{31}} - \frac{J_{13}J_{24}\kappa_{nl}}{J_{21} + J_{22}\kappa_{nl}} - \frac{J_{12}J_{24}J_{32}\kappa_{nl}}{2J_{31}(J_{21} + J_{22}\kappa_{nl})}\right)^{-1}. \tag{4.7}$$

Applying $\kappa_{nl} \to 0$, the upper buckling load corresponding with the bifurcation point of toroidal shell segments can be attained by

$$r_0^{up} = J_{11}/[J_{16} - J_{12}J_{34}/(2J_{31})]. \tag{4.8}$$

Investigating the upper buckling load with all buckling modes, the achieved minimum value in the case of compressive load and maximum value in the case of tensile load is called critical buckling load r_{cr}.

The maximal deflection – nonlinear amplitude relation is expressed from Eqs. (4.4)–(4.6), as

$$\frac{W_{\max}}{h} = \frac{1}{h}\left[\frac{J_{32}(J_{24}\kappa_{nl}r_0 - J_{23}\kappa_{nl})}{2J_{31}(J_{21}+J_{22}\kappa_{nl})} + \frac{\kappa_{nl}}{2} + \left(\frac{J_{24}\kappa_{nl}r_0 - J_{23}\kappa_{nl}}{J_{21}+J_{22}\kappa_{nl}}\right)^{1/2} - r_0\frac{J_{34}}{2J_{31}}\right]. \tag{4.9}$$

Combining Eqs. (4.7) and (4.9), the relation between maximal deflection – compressive or tensile load of shell can be numerically investigated.

5. Comparison examination, numerical investigations and discussions

In this section, the following consents are introduced:

- For the case of compressive load, the compressive load $r_0^c = r_0$, and the critical compressive buckling load $r_{cr}^c = r_{cr}$.
- For the case of tensile load, the tensile load $r_0^t = -r_0$, and the critical tensile buckling load $r_{cr}^c = -r_{cr}$.

In Table 1, the critical compressive buckling loads of simply-supported FG-GRC laminated cylindrical shells (without auxetic core) are validated by comparing with the publication of SHEN and XIANG [22] which uses the nonlinear higher-order shear deformation theory with the two-step perturbation method. The validation cases are compared and acceptable agreements are observed in this study. It seems that for thick shells ($R/h = 20$) the differences between the results of the Donnell shell theory (present results) and those of higher-order shear deformation theory (SHEN and XIANG [22]) are clearly observed.

Table 1. Comparisons of critical axial compressive buckling load $\bar{r}_{cr}^c = r_{cr}^c h 2\pi R h$ [kN] of FG-GRC laminated cylindrical shells ($R/h = 20$, $h = 2\,\text{mm}$, $T = 300\,\text{K}$).

GRC arrangements	L^2/Rh	Present		SHEN and XIANG [22]	
		FG-X	UD	FG-X	UD
$(0)_{10}$	500	1226.10 (4;4)*	1133.55 (4;4)	1154.36 (4;4)	1087.11 (4;4)
	300	1238.44 (3;4)	1143.80 (3;4)	1167.68 (3;4)	1098.08 (3;4)
	100	1194.79 (2;4)	1107.81 (2;4)	1116.33 (2;4)	1056.72 (2;4)
$(0/90/0/90/0)_S$	500	1226.49 (4;4)	1134.25 (4;4)	1154.83 (4;4)	1087.81 (4;4)
	300	1238.95 (3;4)	1144.63 (3;4)	1168.23 (3;4)	1098.87 (3;4)
	100	1194.88 (2;4)	1108.20 (2;4)	1116.70 (2;4)	1057.20 (2;4)
$(0/90)_{5T}$	500	1228.12 (4;4)	1134.94 (4;4)	1156.27 (4;4)	1088.45 (4;4)
	300	1240.73 (3;4)	1145.39 (3;4)	1169.80 (3;4)	1099.57 (3;4)
	100	1196.04 (2;4)	1108.67 (2;4)	1117.73 (2;4)	1057.66 (2;4)

*the buckling modes $(m;n)$ are presented in the parentheses.

To illustrate the present approach, the toroidal shell segments are considered with $R = 0.5\,\mathrm{m}$, $L = 0.75\,\mathrm{m}$, $a = 2\,\mathrm{m}$, $h = 0.002\,\mathrm{m}$. According to [21–23], the matrix of GRC face sheets is made from Poly methyl methacrylate (PMMA). The material properties of graphene and matrix are applied according to the previous results [21–23]. The PMMA auxetic core are applied by default ($\chi_1 = 2$, $\chi_2 = 0.1$, $\theta = 30^\circ$).

Table 2. The critical compressive and tensile buckling loads of auxetic core toroidal shell segments with different longitudinal radii (MPa, $K_W = 10^7\,\mathrm{N/m^3}$, $K_P = 10^5\,\mathrm{N/m}$, $L = 1.5R$, $R/h = 80$, $h = 4\,\mathrm{mm}$, $h_c = 2\,\mathrm{mm}$, $h_{\mathrm{GRC}} = 1\,\mathrm{mm}$, $(0/90/0/90/0)_S$).

Load type	Shell type	a	UD	FG-X	FG-O
Axial compressive loads	Concave	$-2R$	85.98 (1;3)	86.58 (1;3)	82.52 (1;3)
		$-4R$	140.44 (1;4)	141.42 (1;4)	131.58 (1;4)
	Cylindrical	∞	402.45 (5;6)	399.43 (5;6)	360.44 (5;6)
	Convex	$4R$	429.66 (7;1)	411.46 (7;1)	368.87 (7;1)
		$2R$	430.58 (7;1)	412.33 (7;1)	369.68 (7;1)
Axial tensile loads	Convex	$6R$	1281.64 (1;9)	1271.49 (1;9)	1098.20 (1;10)
		$4R$	826.81 (1;9)	812.50 (1;9)	716.21 (1;10)
		$2R$	532.90 (1;11)	517.17 (1;11)	462.34 (1;11)

The critical compressive and tensile buckling loads of auxetic core toroidal shell segments in the convex, concave and cylindrical forms by applying different longitudinal radii are presented in Table 2. The most interesting phenomenon here is that with convex shells, tensile and compressive critical loads are both obtained, however with cylindrical and concave shells only the compressive critical loads are obtained. The change tendencies of the critical buckling load respecting the longitudinal radius are also different for convex and concave shells. For convex shells, the critical buckling compressive loads increase when the longitudinal radius decreases. Inversely, the critical tensile buckling loads decrease when the longitudinal radius decreases. For the concave shells, the axial compressive buckling loads increase when the absolute values of longitudinal radius increases. In the investigated results, the longitudinal buckling modes are always equal to one for axial compressive loads of concave shells and axial tensile loads for convex shells. For axial compressive loads of convex shells, the circumferential buckling modes are equal to one. Only the cylindrical shell case, both longitudinal and circumferential buckling mode reach high values. The complexity due to the nano-effects of graphene can also be observed when in many cases the critical loads of the UD shell are markedly larger than those of FG-X shell for the sandwich shell. This result is also consistent with results of SHEN [22] for the FG-GRC sandwich shell.

Effects of Graphene distributed laws and Graphene arrangements on the critical compressive and tensile buckling loads of convex and concave solid and auxetic core shells with comparisons of critical buckling loads between solid and auxetic cores shells can be recognized in Table 3. As it can be seen that in all investigated cases the tensile and compressive critical loads of auxetic core shell segments are lightly smaller than those of solid core shell segments. This demonstrates that the auxetic core remarkably reduces the mass without remarkably decreasing the critical load of the shells. Three investigated Graphene arrangements $(0)_{10}$, $(0/90)_{5\mathrm{T}}$, and $(0/90/0/90/0)_{\mathrm{S}}$ with the slight differences of obtained results of critical buckling loads display the lightly orthotropic characteristics of Graphene.

Table 3. Critical buckling loads of toroidal shell segments with solid and auxetic cores (MPa, $K_W = 10^7\,\mathrm{N/m^3}$, $K_P = 10^5\,\mathrm{N/m}$, $L = 1.5R$, $R/h = 80$, $h = 4\,\mathrm{mm}$, $h_c = 2\,\mathrm{mm}$, $h_{\mathrm{GRC}} = 1\,\mathrm{mm}$).

Core type	Graphen distribution law	Graphen arrangement	Compressive loads			Tensile loads
			$a = -4R$	$a = \infty$	$a = 4R$	$a = 4R$
Auxetic core	UD	$(0)_{10}$	140.27(1;4)	402.55(5;6)	429.87(7;1)	825.36(1;9)
		$(0/90)_{5T}$	140.49(1;4)	402.37(5;6)	429.37(7;1)	827.39(1;9)
		$(0/90/0/90/0)_S$	140.44(1;4)	402.45(5;6)	429.66(7;1)	826.81(1;9)
	FG-X	$(0)_{10}$	141.21(1;4)	399.43(5;6)	411.62(7;1)	810.82(1;9)
		$(0/90)_{5T}$	141.49(1;4)	399.25(5;6)	410.94(7;1)	813.45(1;9)
		$(0/90/0/90/0)_S$	141.42(1;4)	399.43(5;6)	411.46(7;1)	812.50(1;9)
	FG-O	$(0)_{10}$	131.34(1;4)	360.53(5;6)	369.25(7;1)	713.07(1;10)
		$(0/90)_{5T}$	131.58(1;4)	360.49(5;6)	368.93(7;1)	716.26(1;10)
		$(0/90/0/90/0)_S$	131.58(1;4)	360.44(5;6)	368.87(7;1)	716.21(1;10)
Solid core	UD	$(0)_{10}$	140.55(1;4)	409.90(5;6)	436.34(7;1)	833.52(1;9)
		$(0/90)_{5T}$	140.77(1;4)	409.72(5;6)	435.85(7;1)	835.56(1;9)
		$(0/90/0/90/0)_S$	140.72(1;4)	409.80(5;6)	436.13(7;1)	834.97(1;9)
	FG-X	$(0)_{10}$	141.49(1;4)	406.71(5;6)	418.10(7;1)	818.88(1;9)
		$(0/90)_{5T}$	141.77(1;4)	406.54(5;6)	417.41(7;1)	821.51(1;9)
		$(0/90/0/90/0)_S$	141.70(1;4)	406.72(5;6)	417.94(7;1)	820.56(1;9)
	FG-O	$(0)_{10}$	131.62(1;4)	367.82(5;6)	375.72(7;1)	719.78(1;10)
		$(0/90)_{5T}$	131.86(1;4)	367.78(5;6)	375.40(7;1)	722.97(1;10)
		$(0/90/0/90/0)_S$	131.85(1;4)	367.73(5;6)	375.34(7;1)	722.92(1;10)

Figure 3 presents the effects of core types, Graphene distribution laws and longitudinal radius on the compressive and tensile postbuckling curves of convex and concave toroidal shell segments. The comparisons of compressive and tensile postbuckling curves between auxetic and solid cores, concave and convex shells, respectively, are shown in Figs. 3a and 3b. Corresponding to the critical load,

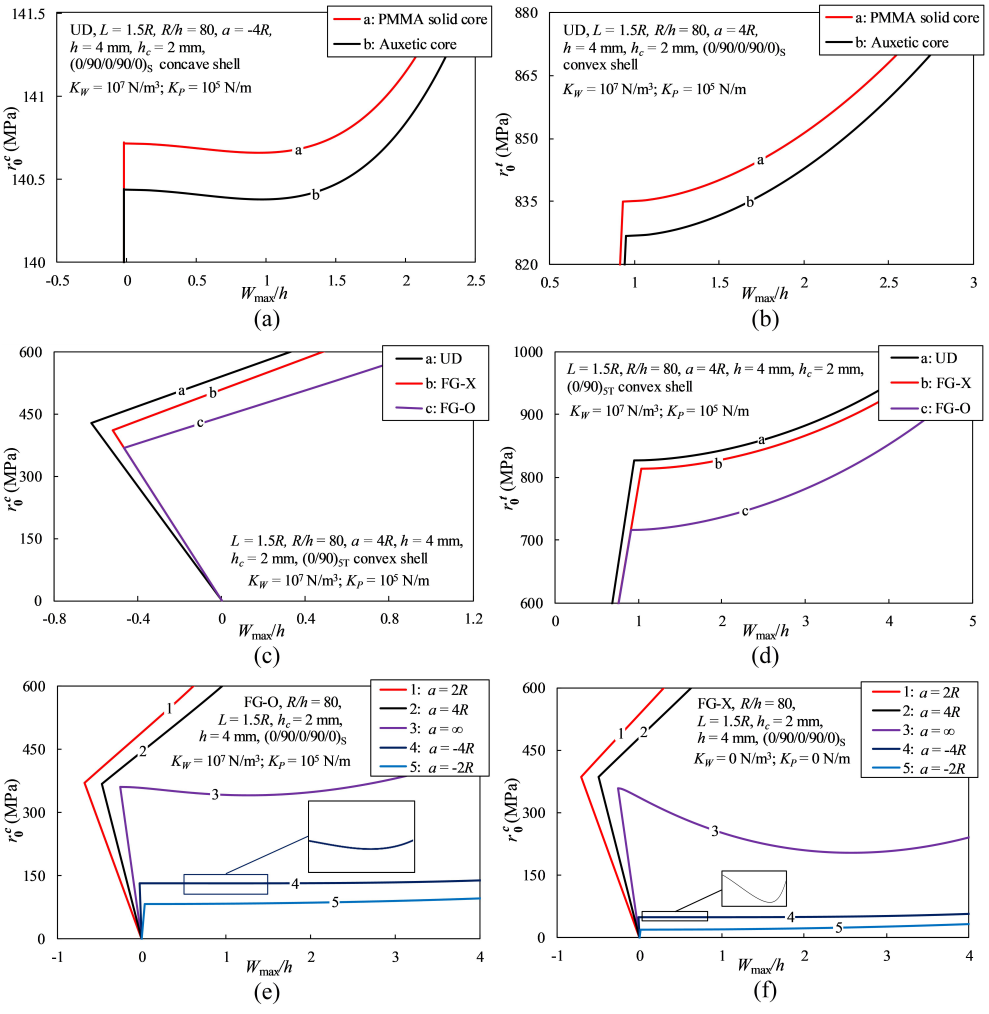

FIG. 3. Effects of core types, Graphene distribution laws and longitudinal radius on the postbuckling curve of shells.

the postbuckling curves of the auxetic core shells are always lower than those of the solid core shells and the fairly similar tendencies of their changes can be observed. It seems that the pre-buckling lines of the solid and the auxetic core shells are overlapping in the case of compressed concave shells.

Effects of Graphene distribution laws on the postbuckling curves of convex auxetic-core shell segments subjected to compressive and tensile loads, respectively, are investigated in Figs. 3a and 3b. These two figures present that the pre-buckling lines of FG-X and FG-O convex toroidal shell segments are overlapping in both cases of compressive and tensile loads. Another interesting ob-

servation is that the postbuckling behavior of the convex toroidal shell segments is almost linear, and this observation can be confirmed again in Figs. 3e and 3f. For the shells subjected to compressive loads, the snap-through phenomenon of the cylindrical shell is the clearest, that of the concave shells is relatively small and does not appear for convex shells.

Table 4. Effect of geometrical parameters of auxetic core on the critical compressive and tensile buckling loads of convex shells with Graphene reinforced face sheets (MPa, $K_W = 10^7\,\mathrm{N/m^3}$, $K_P = 10^5\,\mathrm{N/m}$, $L = 1.5R$, $R/h = 80$, $a = 4R$, $h = 4\,\mathrm{mm}$, $h_c = 2\,\mathrm{mm}$, $h_{\mathrm{GRC}} = 1\,\mathrm{mm}$, $(0/90)_{5T}$).

Auxetic properties	Graphene distribution law	Compressive load	Tensile load
$\chi_1 = 1$, $\chi_2 = 0.1$, $\theta = 15^\circ$	UD	429.80 (7;1)	827.40 (1;9)
	FG-X	411.37 (7;1)	813.45 (1;9)
	FG-O	369.36 (7;1)	716.31 (1;10)
$\chi_1 = 2$, $\chi_2 = 0.1$, $\theta = 30^\circ$	UD	429.37 (7;1)	827.39 (1;9)
	FG-X	410.94 (7;1)	813.45 (1;9)
	FG-O	368.93 (7;1)	716.26 (1;10)
$\chi_1 = 3$, $\chi_2 = 0.1$, $\theta = 45^\circ$	UD	429.26 (7;1)	827.52 (1;9)
	FG-X	410.83 (7;1)	813.59 (1;9)
	FG-O	368.82 (7;1)	716.34 (1;10)

The effects of geometrical parameters of auxetic core on the critical buckling loads of convex shells with Graphene reinforced face sheets are presented in Table 4. Because of the very small stiffnesses of the auxetic core in comparison with the stiffnesses of graphene reinforced face sheets, the effects of geometrical parameters of the auxetic core on both cases of tensile and compressive critical loads of shell segments are unremarkable in all considered examinations. This observation is justifiable with the lightweight cores that are designed to reduce the mass of structures and to increase the eccentricity of two face sheets.

The effects of thickness of auxetic core on the critical compressive and tensile buckling loads of convex shells with Graphene reinforced face sheets are presented in Table 5. In this table, the different core thicknesses are investigated. As it can be seen, the large increase of critical buckling loads can be obtained when the core thicknesses increase. Table 6 demonstrates that the effects of the R/h ratio on the critical compressive and tensile loads of convex toroidal shell segments are remarkable. For both cases of compressive and tensile loads, the critical buckling loads strongly increase with the decreases of R/h ratio.

Effects of auxetic core thickness and R/h ratio on the postbuckling curve of shells are presented in Fig. 4. The figures show that the pre-buckling lines of the convex shells with different auxetic core thicknesses are overlapping in both cases of compressed and tensile loads while the markedly different tendencies of

Table 5. Effects of thickness of core layer on the critical compressive and tensile buckling load of convex toroidal shell segments (MPa, $K_W = 10^7\,\mathrm{N/m^3}$, $K_P = 10^5\,\mathrm{N/m}$, $R = 0.32\,\mathrm{m}$, $a = 4R$, $L = 1.5R$, $h_{\mathrm{GRC}} = 1\,\mathrm{mm}$, $(0)_{10}$).

h_c [mm]	*UD*	*FG-X*	*FG-O*
Compressive load			
0	354.49 (11;1)	355.73 (10;1)	286.45 (12;1)
1	399.47 (8;1)	387.86 (8;1)	338.79 (8;1)
2	429.87 (7;1)	411.62 (7;1)	369.25 (7;1)
Tensile load			
0	628.73 (1;14)	643.96 (1;13)	529.22 (1;15)
1	715.82 (1;11)	718.68 (1;11)	611.72 (1;11)
2	825.36 (1;9)	810.82 (1;9)	713.07 (1;10)

Table 6. Effect of R/h ratio on the critical compressive and tensile buckling loads of convex toroidal shell segments (MPa, $K_W = 10^7\,\mathrm{N/m^3}$, $K_P = 10^5\,\mathrm{N/m}$, $L = 1.5R$, $a = 4R$, $h = 4\,\mathrm{mm}$, $h_c = 2\,\mathrm{mm}$, $h_{\mathrm{GRC}} = 1\,\mathrm{mm}$, $(0)_{10}$).

R/h	Graphene distribution law	Compressive load	Tensile load
60	UD	563.33 (6;1)	1169.82 (1;9)
	FG-X	538.80 (6;1)	1155.38 (1;9)
	FG-O	483.23 (6;1)	994.37 (1;9)
80	UD	429.87 (7;1)	825.36 (1;9)
	FG-X	411.62 (7;1)	810.82 (1;9)
	FG-O	369.25 (7;1)	713.07 (1;10)
100	UD	350.39 (7;2)	650.26 (1;10)
	FG-X	332.71 (7;1)	639.27 (1;10)
	FG-O	301.52 (8;1)	570.66 (1;11)

Table 7. Effects of stiffnesses of foundation on the critical compressive and tensile loads of convex toroidal shell segments (MPa, $L = 1.5R$, $R/h = 80$, $a = 4R$, $h = 4\,\mathrm{mm}$, $h_c = 2\,\mathrm{mm}$, $h_{\mathrm{GRC}} = 1\,\mathrm{mm}$, $(0/90)_{5T}$).

K_W [N/m^3]	K_P [N/m]	Graphene distribution law	Axial compression	Axial tension
0	0	UD	403.04 (7;1)	661.17 (1;9)
		FG-X	384.61 (7;1)	645.93 (1;9)
		FG-O	342.60 (7;1)	555.88 (1;9)
10^7	10^5	UD	429.37 (7;1)	827.39 (1;9)
		FG-X	410.94 (7;1)	813.45 (1;9)
		FG-O	368.93 (7;1)	716.26 (1;10)
1.5×10^7	1.5×10^5	UD	442.54 (7;1)	911.13 (1;10)
		FG-X	424.11 (7;1)	899.79 (1;9)
		FG-O	382.10 (7;1)	795.04 (1;10)

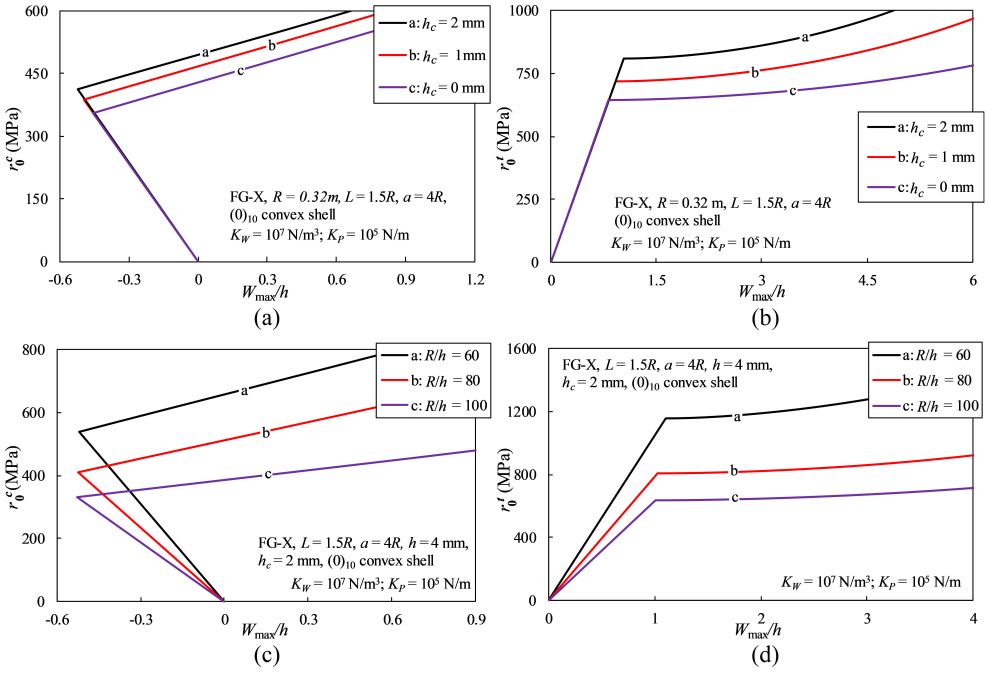

FIG. 4. Effects of auxetic core thickness and R/h ratio on the postbuckling curve of convex toroidal shell segments.

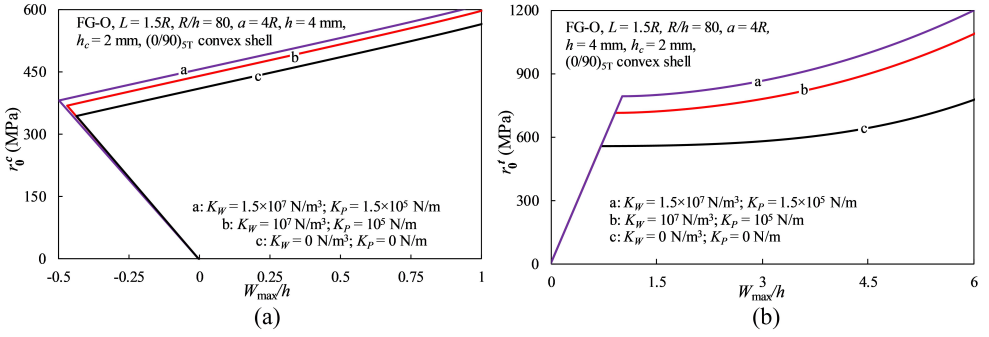

FIG. 5. Effects of elastic foundation stiffnesses on the postbuckling curves of convex and concave shells.

pre-buckling lines and postbuckling curves can be observed with different R/h ratios.

Table 7 shows the effects of shell-foundation interaction on the critical compressive and tensile buckling load of toroidal shell segments with Graphene reinforced face sheets. Clearly that the critical buckling load remarkably decreases when the two stiffnesses of foundation decrease. Figures 5a and 5b present the ef-

fects of shell-foundation interaction on the postbuckling curves of toroidal shell segments. As it can be observed, the compressive postbuckling curves of the convex shells with different foundation stiffnesses are almost parallel. The tensile pre-buckling lines are overlapping, while there occur the small differences of compressed pre-buckling lines with different foundation stiffnesses occur.

6. Conclusion remarks

An approach of governing equations of toroidal shell segments with auxetic core and Graphene reinforced face sheets subjected to axial compressive or tensile loads and surrounded by elastic foundation based upon the nonlinear Donnell shell theory and the homogenization technique for auxetic layers with the Stein and McElman assumption is presented in this paper. The most interesting remarks can be obtained from the present analysis:

- The bifurcation buckling phenomenon appears in both cases of axial tensile and compressive loads for auxetic-core shells. There is no critical buckling load for the concave shells subjected to axial tensile load.
- The postbuckling behavior of the convex shells is almost linear. For convex shells subjected to compressive loads, the snap-through phenomenon of the cylindrical shell is the clearest, that of the concave shells is relatively small and does not appear for convex shells.
- Auxetic core, shell-foundation interaction, Graphene distributions and arrangements, and geometrical parameters largely influence on the nonlinear buckling behavior of toroidal shell segments.

Acknowledgments

This research is funded by University of Transport Technology (UTT) under grant number DTTD2021-03.

References

1. M. Stein, J.A. Mcelman, *Buckling of segments of toroidal shells*, AFAA Journal, **3**, 1704–1709, 1965.
2. M. Koizumi, *The concept of FGM*, Ceramic Transactions, Functionally Gradient Materials, **34**, 3–10, 1993.
3. H. Huang, Q. Han, *Nonlinear elastic buckling and postbuckling of axially compressed functionally graded cylindrical shells*, International Journal of Mechanical Sciences, **51**, 7, 500–507, 2009.
4. H. Huang, Q. Han, *Stability of pressure-loaded functionally graded cylindrical shells with inelastic material properties*, Thin-Walled Structures, **92**, 21–28, 2015.

5. A.H. SOFIYEV, E. SCHNACK, *The stability of functionally graded cylindrical shells under linearly increasing dynamic torsional loading*, Engineering Structures, **26**, 10, 1321–1331, 2004.

6. A. MOOSAIE, *Axisymmetric steady temperature field in FGM cylindrical shells with temperature-dependent heat conductivity and arbitrary linear boundary conditions*, Archives of Mechanics, **67**, 3, 233–251, 2015.

7. A.Y. ALI, H.M. HASAN, *Nonlinear dynamic stability of an imperfect shear deformable orthotropic functionally graded material toroidal shell segments under the longitudinal constant velocity*, Proceedings of the Institution of Mechanical Engineers, Part C: Journal of Mechanical Engineering Science, **233**, 19–20, 6827–6850, 2019.

8. A.H. SOFIYEV, S.E. HUSEYNOV, N. KURUOGLU, *Influence of mixed boundary conditions and heterogeneity on the vibration behavior of orthotropic truncated conical shells*, Archives of Mechanics, **67**, 4, 331–348, 2015.

9. V.H. NAM, N.T. PHUONG, N.T. TRUNG, *Nonlinear buckling and postbuckling of sandwich FGM cylindrical shells reinforced by spiral stiffeners under torsion loads in thermal environment*, Acta Mechanica, **230**, 3183–3204, 2019.

10. V.H. NAM, N.T. PHUONG, C.V. DOAN, N.T. TRUNG, *Nonlinear thermo-mechanical stability analysis of eccentrically spiral stiffened sandwich functionally graded cylindrical shells subjected to external pressure*, International Journal of Applied Mechanics, **11**, 05, 1950045, 2019.

11. N.T. PHUONG, N.T. TRUNG, T.D. KIEN, H.D. TUAN, V.H. NAM, *Nonlinear vibration of full-filled fluid corrugated sandwich functionally graded cylindrical shells*, Journal of Vibration and Control, **27**, 9–10, 1020–1035, 2021.

12. S. IIJIMA, *Helical microtubules of graphitic carbon*, Nature, **354**, 56–58, 1991.

13. H.S. SHEN, *Postbuckling of nanotube-reinforced composite cylindrical shells in thermal environments. Part I: Axially-loaded shells*, Composite Structures, **93**, 8, 2096–2108, 2011.

14. H.S. SHEN, *Postbuckling of nanotube-reinforced composite cylindrical shells in thermal environments. Part II: Pressure-loaded shells*, Composite Structures, **93**, 10, 2496–2503, 2011.

15. Z.X. LEI, L.W. ZHANG, K.M. LIEW, J.L. YU, *Large deflection geometrically nonlinear analysis of carbon nanotube-reinforced functionally graded cylindrical panels*, Computer Methods in Applied Mechanics and Engineering, **273**, 1–18, 2014.

16. Z.X. LEI, L.W. ZHANG, K.M. LIEW, J.L. YU, *Postbuckling of carbon nanotube-reinforced functionally graded cylindrical panels under axial compression using a meshless approach*, Computer Methods in Applied Mechanics and Engineering, **268**, 1–17, 2014.

17. Z.X. LEI, L.W. ZHANG, K.M. LIEW, J.L. YU, *Dynamic stability analysis of carbon nanotube-reinforced functionally graded cylindrical panels using the element-free kp-Ritz method*, Composite Structures, **113**, 328–338, 2014.

18. M.H. HAJMOHAMMAD, R. KOLAHCHI, M.S. ZAREI, M. MALEKI, *Earthquake induced dynamic deflection of submerged viscoelastic cylindrical shell reinforced by agglomerated CNTs considering thermal and moisture effects*, Composite Structures, **187**, 498–508, 2018.

19. V.H. Nam, N.T. Trung, N.T. Phuong, V.M. Duc, V.T. Hing, *Nonlinear torsional buckling of functionally graded carbon nanotube orthogonally reinforced composite cylindrical shells in thermal environment*, International Journal of Applied Mechanics, **12**, 7, 2050072, 2020.

20. K.S. Novoselov, A.K. Geim, S.V. Morozov, D. Jiang, Y. Zhang, S.V. Dubonos, I.V. Grigorieva, A.A. Firsov, *Electric field effect in atomically thin carbon films*, Science, **306**, 666–669, 2004.

21. H.S. Shen, Y. Xiang, F. Lin, *Nonlinear bending of functionally graded graphene reinforced composite laminated plates resting on elastic foundations in thermal environments*, Composite Structures, **170**, 80–90, 2017.

22. H.S. Shen, Y. Xuang, *Postbuckling behavior of functionally graded graphene-reinforced composite laminated cylindrical shells under axial compression in thermal environments*, Computer Methods in Applied Mechanics and Engineering, **330**, 64–82, 2018.

23. H.S. Shen, Y. Xiang, *Postbuckling of functionally graded graphene-reinforced composite laminated cylindrical shells subjected to external pressure in thermal environments*, Thin-Walled Structures, **124**, 151–160, 2018.

24. L.N. Ly, N.T. Phuong, V.H. Nan, N.T. Trung, V.M. Duc, *An analytical approach of nonlinear thermo-mechanical buckling of functionally graded graphene-reinforced composite laminated cylindrical shells under compressive axial load surrounded by elastic foundation*, Journal of Applied and Computational Mechanics, **6**, 2, 357–372, 2020.

25. Y. Kiani, *Buckling of functionally graded graphene reinforced conical shells under external pressure in thermal environment*, Composites Part B: Engineering, **156**, 128–137, 2019.

26. Y. Kiani, *NURBS-based isogeometric thermal postbuckling analysis of temperature dependent graphene reinforced composite laminated plates*, Thin-Walled Structures, **125**, 211–219, 2018.

27. Y. Kiani, *Isogeometric large amplitude free vibration of graphene reinforced laminated plates in thermal environment using NURBS formulation*, Computer Methods in Applied Mechanics and Engineering, **332**, 86–101, 2018.

28. N.T. Phuong, V.H. Nam, N.T. Trung, V.M. Duc, N.V. Loi, N.D. Thinh, P.T. Tu, *Thermomechanical postbuckling of functionally graded graphene-reinforced composite laminated toroidal shell segments surrounded by Pasternak's elastic foundation*, Journal of Thermoplastic Composite Materials, **34**, 10, 1380–1407, 2021.

29. N.T. Phuong, N.T. T.rung, C.V. Doan, N.D. Thang, V.M. Duc, V.H. Nam, *Nonlinear thermomechanical buckling of FG-GRC laminated cylindrical shells stiffened by FG-GRC stiffeners subjected to external pressure*, Acta Mechanica, **231**, 5125–5144, 2020.

30. N.T. Phuong, V.M. Duc, C.V. Doan, V.H. Nam, *Nonlinear torsional buckling of functionally graded graphene-reinforced composite (FG-GRC) laminated cylindrical shells stiffened by FG-GRC laminated stiffeners in thermal environment*, Polymer Composites, **42,** 6, 3051–3063, 2021.

31. V.H. Nam, N.T. Phuong, H.S. Lanh, V.M. Duc, C.V. Doan, *Nonlinear buckling analysis of stiffened FG-GRC laminated cylindrical shells subjected to axial compressive load in thermal environment*, Mechanics Based Design of Structures and Machines, https://doi.org/10.1080/15397734.2021.1932522, 2021.

32. H. EIPAKCHI, F. MAHBOUBI NASREKANI, *Vibrational behavior of composite cylindrical shells with auxetic honeycombs core layer subjected to a moving pressure*, Composite Structures, **254**, 112847, 2020.

33. Z. XIUFANG, Z. JUNHUA, Z. WEI, C. JIE, *Vibration frequencies and energies of an auxetic honeycomb sandwich plate*, Mechanics of Advanced Materials and Structures, **26**, 23, 1951–1957, 2019.

34. X.K. LAN, S.S. FENG, Q. HUANG, T. ZHOU, *A comparative study of blast resistance of cylindrical sandwich panels with aluminum foam and auxetic honeycomb cores*, Aerospace Science and Technology, **87**, 37–47, 2019.

35. C. LUO, C.Z. HAN, X.Y. ZHANG, X.G. ZHANG, X. REN, Y.M. XIE, *Design, manufacturing and applications of auxetic tubular structures: a review*, Thin-Walled Structures, **163**, 107682, 2021.

36. J.S. HU, B.L. WANG, *Crack growth behavior and thermal shock resistance of ceramic sandwich structures with an auxetic honeycomb core*, Composite Structures, **260**, 113256, 2021.

37. L.N. LY, V.M. DUC, N.T. TRUNG, N.T. PHUONG, D.T. DONG, T.Q. MINH, N.V. TIEN, V.T. HUNG, *An analytical approach to the nonlinear buckling behavior of axially compressed auxetic-core cylindrical shells with carbon nanotube-reinforced face sheets*, Proceedings of the Institution of Mechanical Engineers, Part L: Journal of Materials: Design and Applications, **235**, 10, 2254–2265, 2021.

38. N.V. TIEN, V.M. DUC, V.H. NAM, N.T. PHUONG, H.S. LANH, D.T. DONG, L.N. LY, D. HUNG, T.Q. MINH, *Nonlinear postbuckling of auxetic-core sandwich toroidal shell segments with CNT-reinforced face sheets under external pressure*, International Journal of Structural Stability and Dynamics, doi.org/10.1142/S0219455422500067, 2021.

39. D.D. BRUSH, B.O. ALMROTH, *Buckling of Bars, Plates and Shells*, Mc Graw-Hill, London, 1975.

Received December 17, 2021; revised version May 07, 2022.
Published online June 07, 2022.